Deterministic assembly of a charged quantum dot - micropillar cavity device.

P. Hilaire,[1,*] C. Millet,[2] J.C. Loredo,[2] C. Antón,[2] A. Harouri,[2] A. Lemaître,[2]
I. Sagnes,[2] N. Somaschi,[3] O. Krebs,[2] P. Senellart,[2] and L. Lanco[1,†]

[1] *Université de Paris, Centre for Nanoscience and Nanotechnology (C2N), F-91120 Palaiseau, France*
[2] *Centre for Nanoscience and Nanotechnology (C2N), CNRS, Univ Paris Sud, Université Paris-Saclay, F-91120 Palaiseau, France*
[3] *Quandela, 10 boulevard Thomas Gobert, 91120, Palaiseau, France*

(Dated: April 2, 2020)

Quantum-dot based spin-photon interfaces are highly sought systems to implement deterministic photon-photon gates as well as to generate photonic cluster states. This requires mastering the technological challenge of fully controlling the coupling of a charged quantum dot to a cavity mode. Here, we report on a set of technological and experimental developments that allows doing so. The first ingredient consists in combining the in-situ lithography technique, that allows a deterministic spatial and spectral coupling of the emitter to a pillar cavity mode, with a pre-identification of the quantum dot charge states. The second ingredient relies on the design of an asymmetric tunneling barrier to inject the carrier in the quantum dot and an optical control of the charge occupation probability. We show that we can ensure both a high occupation probability of the charge in the quantum dot and an optimal coupling to the cavity mode. This is demonstrated through second order auto-correlation measurements and by measuring the performance of the device as a bright source of indistinguishable single photons.

The efficient interfacing of single photons to natural or artificial atoms is central to the development of efficient quantum light sources[1,2], quantum repeaters[3,4], photon-photon gates[5,6] as well as for the generation of photonic cluster states[7,8]. Strong atom-photon interactions are commonly obtained by inserting a single atom in an optical resonator to control the spontaneous emission into a well designed optical mode[9,10]. The atom-photon interface can act as an efficient emitter of indistinguishable, single photons[11–13], but also as an efficient single-photon receiver. In the latter case, the atom can be used as a quantum memory to store the photonic state, or to realize various atom-photon, atom-atom or photon-photon gates[5,14,15].

Semiconductor quantum dots (QDs) are excellent artificial atoms, able to emit highly-pure single-photons and to route light at the single-photon level when inserted in cavities[6,16]. Exploiting the spin state of a single charge in the QD, either an electron or a hole, is essential to demonstrate deterministic photon-photon gates and generate highly sought photonic cluster states[17,18], two central features for the scalability of optical quantum technologies.

However, the deterministic fabrication of such singly-charged cavity quantum electrodynamics (cQED) devices is very challenging as it requires fulfilling multiple stringent requirements at the same time. The first one is the optimal spatial and spectral coupling of a singly-charged QD state to a cavity mode. A second challenge is to controllably prepare the QD in the desired charge state, consisting of either an electron or a hole in excess. Finally, the cavity must allow the photons to be efficiently injected and collected after having interacted with the QD. In this respect, pillar microcavities allow for both efficient injection[19–21] and collection of photons[11–13].

Here, we report on a set of experimental and technological methods that result in a high control on the injection of a single charge in a quantum dot, which is at the same time optimally coupled to a micropillar cavity mode. To do so, we make use of an engineered asymmetric band structure that hinders the tunneling of an optically-injected hole out of the QD. An in-plane magnetic field photoluminescence study of the various QD charge states allows us to identify the positively-charged state within the pattern of various emission lines. We define electrically connected micropillar cavities centered on chosen quantum dots, using a cryogenic in-situ lithography step[22,23], during which we measure the positive trion energy transition and tune the cavity frequency accordingly. The quality of the fabricated charged quantum dot-cavity interfaces is evaluated via intensity correlations measurements and by showing the excellent performance of the device as a single-photon source.

This paper is organized as follows. In Sec. I, we present the sample structure and the technological procedure. The scheme used to trap a single carrier in the QD is presented in Sec. II. We then discuss the deterministic coupling of the cavity to the trion transition in Sec. IV and evaluate its performances in Sec. V. Finally, the properties of the devices operating as single-photon sources are discussed in Sec. VI.

I. SAMPLE STRUCTURE AND TECHNOLOGICAL PROCEDURE.

The micropillars are fabricated from a planar sample embedding a λ-cavity, surrounded by two distributed Bragg reflectors (GaAs and $Al_{0.9}Ga_{0.1}As$, with 14 and 28 pairs for the top and bottom mirrors respectively). The reduced number of layer pairs in the top mirror allows for a higher output coupling efficiency of the photons emit-

ted by the QD towards the top.

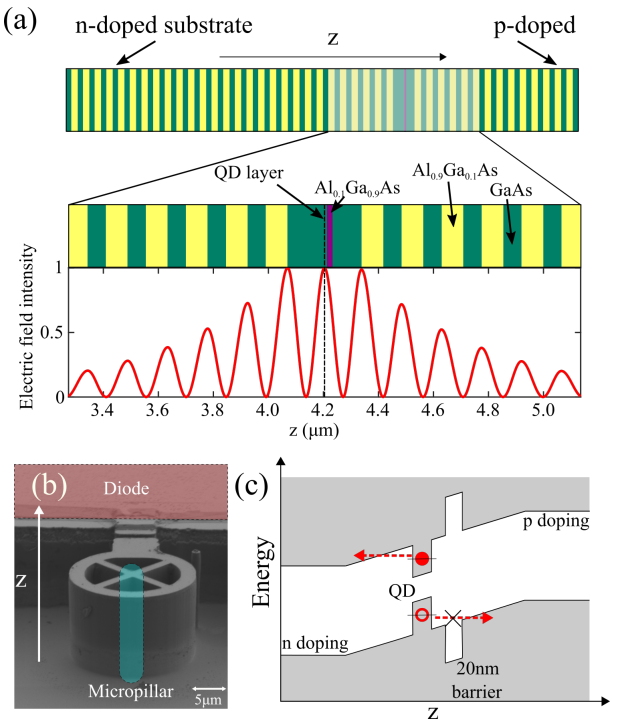

Figure 1. (a) Simulated electromagnetic field intensity inside the micropillar structure. The electromagnetic field is confined at the cavity layer position (green: GaAs layers, yellow: $Al_{0.9}Ga_{0.1}As$ layers, purple: $Al_{0.1}Ga_{0.9}As$ tunneling barrier). (b) Scanning electron microscopy image of a sample. (c) QD + doping structure: the n-doping and p-doping region tilt the forbidden band so that fluctuating charges remain far from the QD, therefore stabilizing the electrical fluctuations. The tunneling barrier reduces the hole tunneling rate.

Fig. 1(a) displays the electromagnetic field intensity calculated by a standard transfer matrix method as a function of the position in the structure (due to its small width, the QD layer was neglected in these simulations). The micropillar structure confines the electromagnetic field with a maximum intensity in its center where the quantum dot is located.

The vertical structure comprises a p-i-n junction[19,24] with a doping density that gradually decreases while approaching the cavity (negative doping for the bottom mirror and positive doping for the top mirror). Such an approach allows minimizing optical losses due to doping in the cavity layer. The structure is connected to an electrically-contacted diode through four ridges and a circular frame as shown in Fig. 1(b).

A well-known technique to control the charge state of QDs is via the bias voltage, which brings the Fermi energy close to a charged QD state[25,26]. Here, we adopt the approach proposed in Ref. 27, based on an asymmetric confinement of an optically-injected electron-hole pair. The λ-cavity consists of a GaAs layer that embeds a single InGaAs QD and a 20-nm thick tunneling barrier of $Al_{0.1}Ga_{0.9}As$, positioned 10nm above the QD layer. The energy levels of the QD and its near environment are schematized in Fig. 1(c), which sketches the energy bands as a function of the vertical position in the cavity layer. The doped regions tilt the bands, allowing the tunneling of carriers out of the quantum dot. Yet the $Al_{0.1}Ga_{0.9}As$ barrier, being placed above the QD layer, is used to strongly increase the tunneling time for a hole trapped in the quantum dot, typically by three orders of magnitude[27], while keeping the electron tunneling time unchanged. The resulting difference in the electron-hole tunneling time allows the trapping of a single hole when optically creating an electron-hole pair.

The micropillar cavities are fabricated using the in-situ lithography technique to center the chosen QDs within the pillar mode[22,23]. This is obtained by measuring the QD position with nanometer-scale accuracy through photoluminescence mapping and by defining a connected pillar cavity centered on the QD during the same step. The cavity diameter is adjusted so that the trion transition is matched to the cavity mode. It is thus essential to be able to identify the QD emitting charge state (neutral exciton, charged exciton, etc) during the in-situ lithography procedure. To do so, we detail the experimental conditions used here to optically trap a hole in Sec. II and discuss how we identify the lines through magnetic field spectroscopy in Sec. III.

II. OPTICAL INJECTION OF A SINGLE-HOLE.

We describe here the optical method used to inject a hole in the quantum dot. The stable QD state is the crystal ground state, here denoted as neutral QD, whose energy levels are represented in the left part of Fig. 2 (a).

An electron-hole pair can be generated by resonantly pumping the exciton (ω_X) or other discrete transitions (such as "p-shell" transitions or LO-phonon-assisted transitions) here denoted as quasi-resonant (QR) transitions with energy $\omega_{QR} > \omega_X$[28,29]. Here, this is done using a CW laser at a wavelength around $\lambda_{QR} = 901$nm as depicted in the left panel of Fig. 2(b).

When an exciton is quasi-resonantly created in the QD, the electron and the hole excess energy non-radiatively decays (in typically less than 100ps[30]) and the system reaches the lower exciton level, as shown in the middle panel of Fig. 2(b). If the exciton radiatively recombines by emitting a photon, the QD then returns to its ground state. This generation-recombination cycle keeps going until an optically-created electron eventually tunnels out towards the n-doped electrical contact before the radiative recombination occurs. Due to the $Al_{0.1}Ga_{0.9}As$ barrier, the remaining hole is confined in the QD for a longer time, during which the QD is in the desired positively-charged state.

The addition of a hole in the QD induces a strong modification of the electric environment by Coulomb interaction, modifying all the discrete energy levels of the QD, as illustrated in the right-hand side of Fig. 2(a).

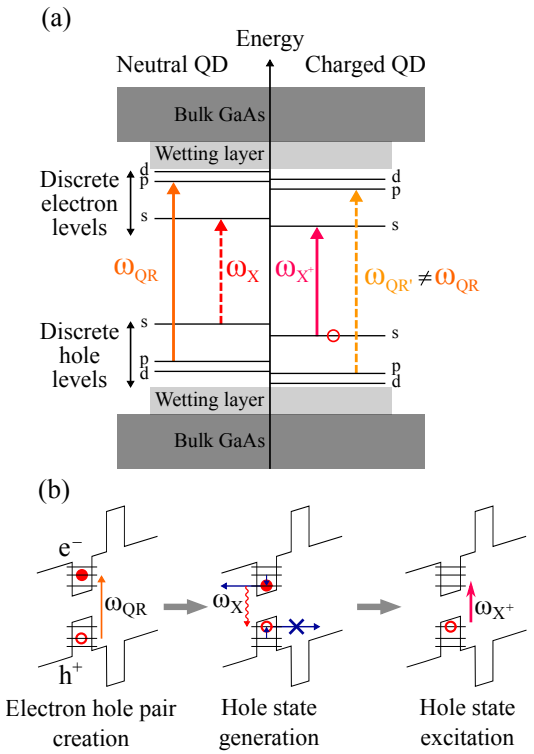

Figure 2. (a) Sketch comparing the energy levels of a neutral QD and a singly-charged QD. The resonant trion transition energy ω_{X+} is different from the exciton transition energy ω_X ($\omega_{X+} \neq \omega_X$) and the p-shell transition energies of a charged QD are also different from a neutral QD: $\omega_{QR'} \neq \omega_{QR}$. (b) Hole trapping scheme using quasi-resonant excitation. Left panel: the QD stable state is the crystal ground state. A quasi-resonant laser creates an electron-hole pair by exciting a p-shell transition (ω_{QR}). Middle panel: If the electron tunnels out the QD before radiative recombination with the hole, it generates of a single hole QD state. Right panel: the QD can then be resonantly excited by a laser with energy ω_{X+} corresponding to the trion transition.

The positively-charged QD thus presents a different energy structure than the neutral one, a feature that applies to LO-phonon assisted and p-shell optical transitions as well. Thus, the incoming frequency ω_{QR} does not induce any optical excitation when a hole is confined. This allows trapping only a single hole in the quantum dot as shown later on.

III. CHARGE STATE IDENTIFICATION.

In order to define the pillar cavity diameter to match the trion transition of a positively-charged QD, we have developed spectroscopy tools to identify the QD energy levels in the experimental conditions of the in-situ lithography - i.e. non-resonant excitation around 850 nm. With above-band excitation, the emission spectrum of the QD presents emission lines corresponding to both the neutral and charged energy levels. To be able to distinguish these lines, we have performed a systematic study of the QD emission under an in-plane magnetic field.

The trion transitions with and without magnetic field are sketched respectively in the top-right and top-left panels of Fig. 3(a). At zero external magnetic field (top-left panel of Fig. 3(a)), a trion radiatively decays into the hole state by emitting a circularly-polarized photon with either a right-handed or a left-handed helicity. There are therefore two trion transitions that are energy degenerate. When an in-plane magnetic field is applied, it induces a Zeeman splitting between the hole states and the trion states, and it also modifies the system eigenstates and thus the optical selection rules, as illustrated in the top-right panel of Fig. 3(a). For a high in-plane magnetic field ($B_x > 1$T typically), a trion decays into a hole by emitting a single photon with 4 combinations of linear polarizations and energies.

The neutral exciton transitions with and without magnetic field are sketched respectively in the bottom-right and bottom-left panels of Fig. 3(a). At zero external magnetic field, the two exciton states $|e_X\rangle$ and $|e_Y\rangle$ radiatively decay into the same ground state $|g\rangle$ (the neutral state) by emitting a photon with linear polarization X and Y, respectively. An in-plane magnetic field increases the energy splitting between the two excited states and modifies the polarization of the emitted photons to either horizontal or vertical. Note that even in the case of a strong in-plane magnetic field, an exciton decays by emitting a single photon with only two combinations of linear polarizations and energies and thus, can be discriminated from the trion transition.

The bottom panel of Fig. 3(b) shows a typical photoluminescence spectrum obtained on a QD in a planar cavity sample, under non resonant excitation ($\lambda_{NR} = 850$nm) and without any applied magnetic field. There are three dominant transitions observed, at 925.1nm, 925.3nm and 925.7nm; the lower intensity transition (at 925.5nm) is related to another QD spatially close to the one under study.

When an in-plane magnetic field is applied, the QD transitions split as seen in the middle panel of Fig 3(b), which displays the evolution of the photoluminescence spectrum under an increasing in-plane magnetic field intensity. At $B_x = 4$T and above, all the observed peaks are split into two transitions. At high magnetic field, all the observed QD transitions are also blue-shifted, due to the diamagnetic shift[31]. The trion transition splits into four different transitions; however, the limited spectrometer resolution impedes the visualization of such effect which is revealed by polarization analysis instead.

The top panel of Fig. 3(b) displays the polarization-resolved photoluminescence for the same QD at $B_x = 4$T. The red (green) curve corresponds to the horizontally-polarized (vertically-polarized) photoluminescence. The horizontal (vertical) polarization peak centers are highlighted by red (green) vertical lines.

Let us first consider the higher wavelength transi-

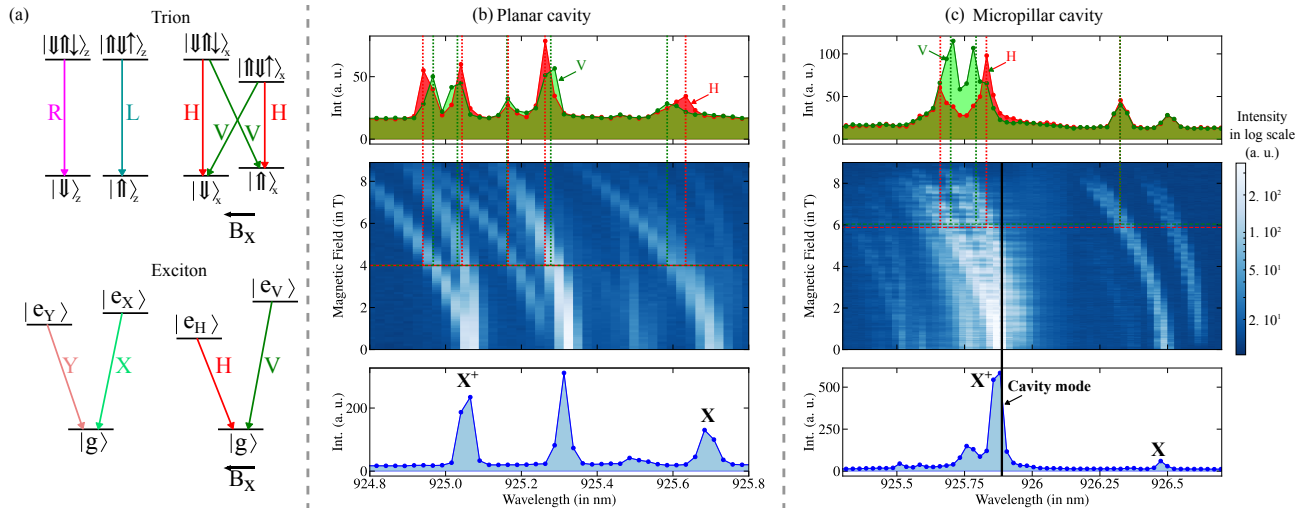

Figure 3. (a) Optical selection rules of a trion (top) and an exciton (bottom), with (right) and without (left) external transverse magnetic field. (b, c) QD photoluminescence under an 850-nm non-resonant laser in (b) a planar cavity sample before etching and (c) after the pillar etching ((b) and (c) represent photoluminescence from different quantum dots.). Bottom panel: without any applied external magnetic field and polarization selection. Middle panel: under varying in-plane magnetic field. Top panel: with strong in-plane magnetic field ((b) $B_x = 4$T and (c) $B_x = 6$T) measured with horizontal (red) and vertical (green) polarizations. (In the middle panel of (c), a waveplate is also rotated before the spectrometer, during the magnetic field scan, to obtain polarization resolution.)

tion (925.7nm at $B_x = 0$T) from the bottom panel of Fig. 3(b). The magnetic field scan and the polarization analysis show that it is split in two transitions with orthogonal linear polarizations. This is the expected behavior for an exciton[32].

As can be seen in the middle and top panels of Fig. 3(b), the lower wavelength transition (925.1nm at $B_x = 0$T) analysis shows that it is split in four transitions with different energies and polarizations: the highest and lowest have the same horizontal polarizations and are orthogonal to the two intermediate vertically-polarized transitions. This state is therefore identified as a trion, as this is the behavior expected from the polarization selection rules of Fig. 3(a).

We note that the center transition (925.3nm at $B_x = 0$T) analysis is also split in four transitions with similar polarizations as the QD trion. However, there is a clear asymmetry in the photoluminescence intensity for these four transitions. This feature may be explained by the X^{2+} states, corresponding to a QD charged with two holes[33,34].

IV. POSITIVE TRION-OPTICAL MODE COUPLING

We have conducted the above emission analysis on a large number of QDs on the planar cavity sample used to fabricate the pillars. Such a systematic study allows us to identify the various QD transitions in a fingerprint-type analysis[35]. During the in-situ lithography step, while no magnetic field is applied, we can thus precisely identify the lines corresponding to the charged-QD and tune the pillar cavity mode energy to the right transition. After the in-situ lithography procedure, and the following etching and electrical contacting steps[22,23], we return to magneto-optics measurements to demonstrate the coupling of the positively charged trion transition to the cavity mode.

Fig. 3(c) presents the emission spectrum of a QD inserted in a micropillar under above-band excitation. The bottom panel represents the photoluminescence at $B_x = 0$T, displaying discrete peaks: the most intense peak corresponds to the QD transition that is coupled to the fundamental cavity mode. The middle panel of Fig. 3(c) shows the evolution of the photoluminescence when increasing the magnetic field. The top panel of Fig. 3(c) represents the photoluminescence collected for an external transverse magnetic field of approximately 6T in H and in V polarizations. The QD transition that is in resonance with the fundamental cavity mode is characterized by four Zeeman-split transitions as expected for a positive trion transition.

V. PERFORMANCES OF THE HOLE TRAPPING

In the following, the hole trapping scheme performances, namely the single-hole occupation probability and the single-hole trapping time, are evaluated by observing the resonance fluorescence signal on multiple QD-cavity devices. In addition to the quasi-resonant laser used for the hole trapping, we use a second laser in res-

onance with the trion transition, i.e. at the energy ω_{X^+} ($\neq \omega_X$) with typical power $P_{X^+} \approx 0.1-3$nW, to measure the resonance fluorecence of the charge QD.

To suppress the resonant laser and only collect the emitted single photons, we use a cross-polarized setup where the trion transition is resonantly excited with a horizontally-polarized resonant laser. The resonance fluorescence is collected through a vertical polarizer that filters out the resonant laser (the quasi-resonant laser is spectrally filtered). The 15-ps pulse laser in resonance with the trion transition induces Rabi oscillations between the hole and the trion state[36–38] depending on the pulse area P_{X^+}. Note that single photons are emitted only if the hole is trapped in the QD. Therefore, the detection of a single photon ensures that a single hole is confined in the QD.

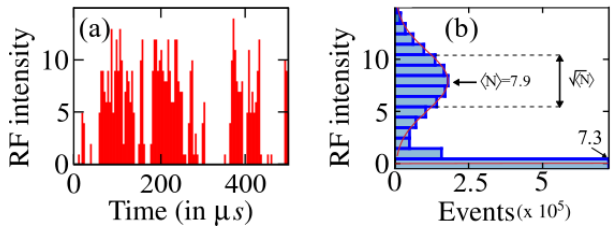

Figure 4. (a) Time trace recording the number of single-photons detected per time bin $\Delta t = 4\mu$s (with $P_{QR} = 50\mu$W and P_{X^+} corresponding to π-pulse). (b) Histogram of the number of time bins corresponding to a given number of detected photons, during an acquisition time of approximately 10s. It represents the intensity distribution of the single-photon source and displays the addition of a high zero detected photon probability and a gaussian distribution (with $\langle N \rangle = 7.9$ photons $/\Delta t$ and a width of $\sigma = 2.8 (= \sqrt{\langle N \rangle})$).

Fig. 4(a) represents the time trace of the cross-polarized resonance fluorescence intensity emitted by one QD-pillar device, observed with a quasi-resonant power of $P_{QR} = 50\mu$W, a π-pulse resonant excitation and a time bin of $\Delta t = 4\mu$s. It evidences a clear blinking of the QD occupation levels between charged and neutral states. This is further shown in the histogram of Fig. 4(b) representing the distribution of the number of detected events per time bin Δt. The histogram shows the presence of two states for the QD, a bright and dark state, the latter corresponding to any case where the QD does not trap a single hole, leading to the absence of detected photons and thus $N = 0$ photon per time bin. The signal corresponding to the bright state shows a typical Poisson distribution, centered on $\langle N \rangle = 7.9$ photons per time bin, with a width given by the square root of the average value.

From this histogram, comparing the area of the bright and dark state events, we can deduce a hole occupancy of around 60%. Note that there is another signal at $N = 1$ photon per time bin which prevents an accurate determination of the hole occupation probability using this method. We identify this noise to a background signal arising from the imperfect laser rejection and the detector dark counts. To precisely determine the hole occupation probability together with the hole trapping time, we now turn to second-order correlations of the cross-polarized resonance fluorescence as pioneered by Ref. 39. A typical auto-correlation measurement is displayed in Fig. 5(a), where the two photon coincidence histogram is plotted for different detection delays. The peaks are separated by a delay $T_R = 1/f$, where $f = 82$MHz is the laser repetition rate. In Fig. 5(a), the continuous background between two peaks is due partly to the detector dark counts, but mainly to imperfect filtering of the quasi-resonant laser.

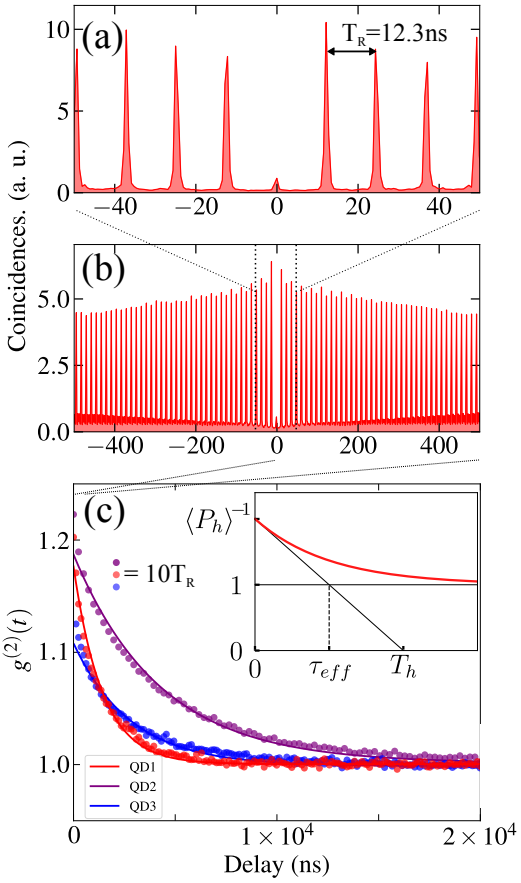

Figure 5. (a,b) Coincidence measurement observed at (a) short and (b) intermediate timescales. (c) Intensity auto-correlations $g^{(2)}(t)$ of the same set of data (QD1) and for two other devices (QD2 and QD3), for even longer timescale and with time bin $\Delta t = 10T_R$. The decay is fitted by an exponential curve (in red). The inset illustrates how the hole occupation probability $\langle P_h \rangle$ and the hole trapping time T_h can be deduced from these correlation measurements.

Fig. 5(b) shows the same set of data for longer delays, at which we can observe that the envelope of the peaks is decaying. Fig. 5(c) shows the intensity auto-correlations $g^{(2)}(t)$ at even longer times (integrated with a time bin $\Delta t = 10T_R$) with the same set of data (QD1 in red)

and for two other devices (QD2 and QD3 respectively in purple and blue). Here, the large binning blurs out the peaks which were visible in Fig. 5(a) and (b), as well as the zero-delay antibunching. The correlation measurements evidence an exponential decay for the three devices, originating from the on/off fluctuations of the hole state in the QD. This effect is used to extract the hole confinement characteristics, as is shown in the following.

The auto-correlation function $g^{(2)}(t)$ can be interpreted as the probability to detect a photon in a detector (denoted APD1) at time t, conditioned to the detection at time $t = 0$ of a photon in the other detector (denoted APD0) normalized by the uncorrelated probability of detecting a photon at any time:

$$g^{(2)}(t) = \frac{P(\text{APD1}, t|\text{APD0}, 0)}{P(\text{APD1})} \tag{1}$$

Immediately after a photon detection in APD0, the probability that a hole is trapped in the QD is $P_h(0) = 1$ and the detection of a photon in APD1 is thus more probable shortly after this first detection.

To interpret the dynamics of the charge state, we develop a model using two states: "0" (the crystal ground state, with zero excess charge) and "h" (the hole state)[39]. The CW quasi-resonant laser transfers the quantum dot state from "0" to "h" at a rate γ (which directly depends on the quasi-resonant power P_{QR}, used to populate the single hole state). Conversely, the hole can tunnel out from the quantum dot with a tunneling time T_h. The occupation probability of the empty state and the charged states are denoted $P_0(t)$ and $P_h(t)$ respectively, with $P_0(t) + P_h(t) = 1$. Their rate equations are:

$$\begin{aligned} \frac{dP_h(t)}{dt} &= \gamma P_0(t) - \frac{1}{T_h} P_h(t) \\ \frac{dP_0(t)}{dt} &= -\gamma P_0(t) + \frac{1}{T_h} P_h(t) \end{aligned} \tag{2}$$

We now assume that at time $t = 0$, a single photon emitted by the QD is detected. A hole is thus trapped inside the quantum dot with a probability $P_h(0) = 1$ and the hole occupation probability evolution is given by:

$$P_h(t) = (1 - \langle P_h \rangle) e^{-\frac{t}{\tau_{eff}}} + \langle P_h \rangle \tag{3}$$

with $\langle P_h \rangle = P_h(\infty) = \gamma/(\gamma + \frac{1}{T_h})$, the average hole occupation probability, and $\tau_{eff} = \left(\gamma + \frac{1}{T_h}\right)^{-1}$, the effective time characterizing the charge dynamics.

In this model, the enveloppe of the auto-correlation function is given by:

$$g^{(2)}(t) = \frac{P_h(t)}{\langle P_h \rangle} = \left(\frac{1}{\langle P_h \rangle} - 1\right) e^{-t/\tau_{eff}} + 1 \tag{4}$$

Therefore, it is possible to extract the hole occupation probability and the hole tunneling time through these auto-correlation measurements, as illustrated in the inset of Fig. 5(c): the enveloppe of the $g^{(2)}(t)$ varies from $1/\langle P_h \rangle$ at zero delay to 1 in a characteristic time τ_{eff}. In addition, its tangent at zero-delay crosses the x-axis at $t = T_h$.

We include the effect of small background noise and obtain the real auto-correlation function of the quantum dot light source $g^{(2)}(t)$ deduced from the experimental one $g^{(2)}_{exp}(t)$. Let P_{QD} be the probability that a photon detected is originated from the quantum dot and $1 - P_{QD}$, the probability that it is originated from bad laser filtering or dark counts. The relation between $g^{(2)}_{exp}(t)$ and $g^{(2)}(t)$ is given by:

$$g^{(2)}(t) = \frac{g^{(2)}_{exp}(t) - 2(1 - P_{QD}) + (1 - P_{QD})^2}{P^2_{QD}} \tag{5}$$

In Fig. 5(c) and 6(a,b), the corrected $g^{(2)}(t)$ is displayed, from which the occupation probability and the hole trapping time can be directly extracted using the fit with Eq. 4.

The dependence of the hole trapping time and hole occupancy is now studied as a function of the quasi-resonant (P_{QR}) and resonant (P_{X^+}) laser powers. Fig. 6(a) shows the dependence of correlation measurements with respect to P_{QR}, with P_{X^+} fixed to π-pulse. Similarly, Fig. 6(b) shows the dependence of correlation measurements with P_{X^+}, with P_{QR} fixed to 50µW. These two figures show that the correlation timescales and the zero-delay value both depend on the resonant and quasi-resonant laser powers.

For all P_{QR} and P_{X^+}, the resulting correlations are fitted with an exponential decay, to extract the hole occupation probability $\langle P_h \rangle$ and the hole trapping time T_h, that are displayed in Fig. 6(c) and (d), respectively. As expected, $\langle P_h \rangle$ is increasing with P_{QR}: it reaches $\langle P_h \rangle = 85 \pm 1\%$ for QD1. The hole trapping time is higher than 20µs except for $P_{QR} > 100$µW. This shows that T_h is always higher than the typical hole spin lifetime at zero magnetic field (which is generally around 1µs)[40].

We note that T_h and $\langle P_h \rangle$ should not vary with the resonant power according to the simple model considering only the zero and one hole states. In addition, the hole trapping time T_h should be constant, equal to the hole tunneling time. The observed deviation from our model can be explained if we consider the possibility of generating a two-hole state: due to the pumping by the two lasers, it is possible to generate a second electron-hole pair when a single hole is already present in the QD and, if the electron tunnels out of the quantum dot, to obtain a two-hole state. This limits the hole occupation probability and reduces the hole trapping time in the strong pumping regime.

Finally, Fig. 6(e) shows the evolution of the polarized brightness B_p as a function of the measured hole occupation probability. B_p is defined as the probability per excitation pulse to detect a polarized single photon after the first lens[2]. It is measured by dividing the measured count rate C, by the laser repetition rate f, the

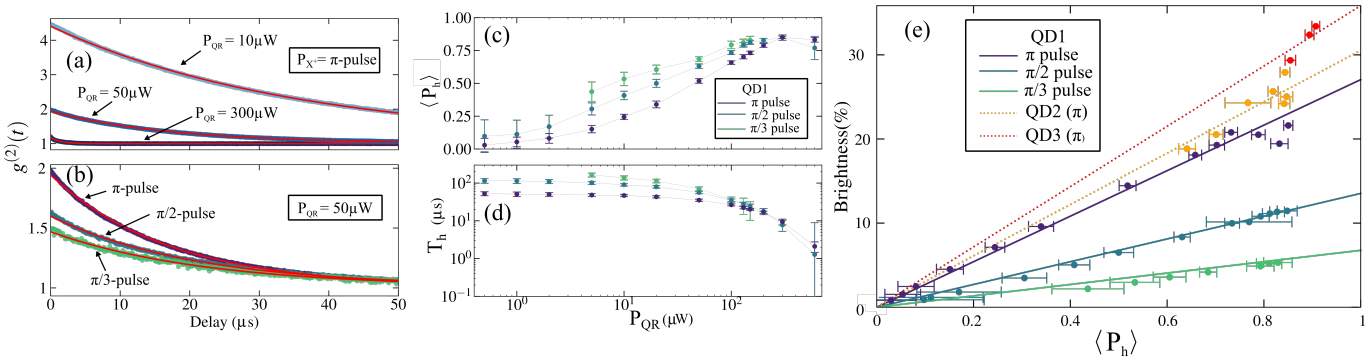

Figure 6. (a, b) Auto-correlation measurements for (a) varying non resonant powers P_{QR} (with fixed P_{X+} corresponding to π-pulse) and (b) varying resonant power P_{X+} (with fixed $P_{QR} = 50\mu$W). Red curves are exponential decay fits. (c,d) Extracted (c) hole occupation probability $\langle P_h \rangle$ and (d) trapping time T_h as a function of the non resonant P_{QR} and resonant P_{X+} powers. (e) Polarized brightness dependence on the hole occupation probability. Points are experimental data that are fitted with solid linear lines. The brightness measurement error bars are not represented on this panel but are typically of $\pm 5\%$.

setup transmission T (evaluated by independant component transmission measurements), and the detector efficiency η_{det}:

$$B_p = \frac{C}{fT\eta_{det}} \tag{6}$$

As expected, the measured brightness is proportional to the hole occupation probability : the measured B_p corresponding to π, $\pi/2$, $\pi/3$ pulses are fitted altogether by 3 linear functions with relative slopes $s_\pi = 26.2\%$, $s_{\pi/2} = s_\pi \cos^2(\pi/2)$ and $s_{\pi/3} = s_\pi \cos^2(\pi/3)$ (the $\cos^2$ takes into account the partial population inversion to the trion state for $\pi/2$ and $\pi/3$ pulses).

The probability that an intracavity photon escapes the cavity through the top mirror is called the output coupling and is measured by independent reflectivity measurements and shows values around $\eta_{top} = 85 \pm 5\%$. For QD1, the maximum observed brightness is 21% and corresponds to a $85 \pm 1\%$ occupation probability.

These experiments have been repeated on two other devices, QD2 and QD3. In these cases, a remarkably high polarized brightness has been measured: $B_p = 28 \pm 5\%$ for QD2 and $B_p = 33 \pm 5\%$ for QD3. They both show a similarly high hole occupation probability with $\langle P_h \rangle = 85 \pm 1\%$ for QD2 and with $\langle P_h \rangle = 91 \pm 1\%$ for QD3.

VI. PERFORMANCES OPERATING AS SINGLE-PHOTON SOURCES.

Finally, the quantum properties of the cQED devices are investigated by assessing performances as single photon sources. The single-photon purity is evaluated by the short timescale zero-delay intensity correlations, measuring the $g^{(2)}(0)$ with a Hanbury-Brown and Twiss (HBT) experiment[41]. A spectral filter (30pm bandwidth) is inserted in the collection setup to further suppress the spectrally-wide excitation laser and phonon side band emission. The results obtained on QD1 show a good

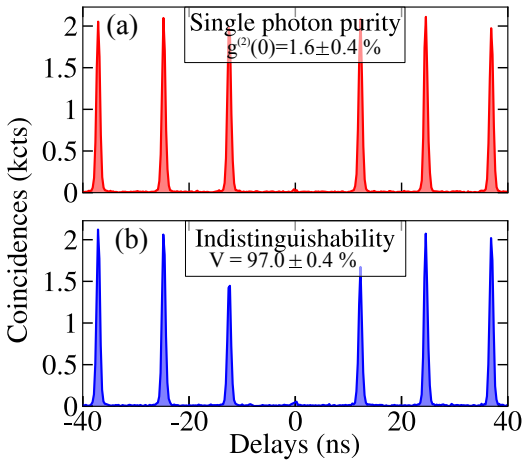

Figure 7. Quantum performances of the cQED devices. Single photon purity and photon indistinguishability are estimated by HBT (a) and HOM (b) experiments for device QD1 (with a Fabry-Pérot etalon to better suppress the reflected laser).

single-photon purity $g^{(2)}(0) = 1.6 \pm 0.4\%$ as displayed in Fig. 7(a).

The single-photon indistinguishability is evaluated by coalescence measurements via the Hong-Ou-Mandel (HOM) effect[42]. This is performed experimentally using a path-unbalanced Mach-Zender interferometer[43] where the difference of delay between the two arms is set to be equal to the laser period T_R. Therefore, two single-photons generated by two immediately separated laser pulses can interfere. Fig. 7(b) displays the experimental results obtained on QD1: the measured photon indistinguishability is at the state of the art with a raw HOM visibility $V = 97 \pm 0.4\%$.

VII. CONCLUSION

We have provided a set of experimental and technological tools for the controlled realization of singly-charged QD-photon interfaces. The key points of our work are: facilitating the hole confinement with a tunneling barrier; using in-plane magnetic-field spectroscopy to identify the trion transition under non-resonant excitation; defining the cavities with the proper geometry to match the targeted trion transition using the in-situ lithography technique; and optically injecting a single hole with a quasi-resonant pumping scheme. The resulting charged QD-photon interfaces have then been used to monitor in real time the jumping of the hole in and out of the quantum dot on a time scale of tens of microseconds. Autocorrelation measurements give access to the hole tunnelling time, and to the hole occupation probability $\langle P_h \rangle$ which has been shown to reach large values, between 85% and 91%, for multiple devices. The high-quality of the spin-photon interfacing devices was evidenced by state-of-the-art performances of the devices operated as bright sources of pure and indistinguishable photons.

ACKNOWLEDGMENTS

This work was partially supported by the ERC PoC PHOW, the French Agence Nationale pour la Recherche (grant ANR SPIQE and ASTRID LIGHT), the QuantERA network (project HIPHOP), the French RENATECH network and a public grant overseen by the French National Research Agency (ANR) as part of the Investissements d'Avenir programme (Labex NanoSaclay, reference ANR-10-LABX-0035). J.C.L. and C.A. acknowledge support from Marie Skłodowska-Curie Individual Fellowships SMUPHOS and SQUAPH, respectively.

* present address: paulhilaire@vt.edu
† loic.lanco@univ-paris-diderot.fr

[1] M. Varnava, D. E. Browne, and T. Rudolph, Physical Review Letters **100**, 060502 (2008).
[2] P. Senellart, G. Solomon, and A. White, Nature nanotechnology **12**, 1026 (2017).
[3] H. J. Kimble, Nature **453**, 1023 (2008).
[4] J. Borregaard, A. S. Sørensen, and P. Lodahl, Advanced Quantum Technologies **2**, 1800091 (2019).
[5] K. Koshino, S. Ishizaka, and Y. Nakamura, Physical Review A **82**, 010301 (2010).
[6] S. Rosenblum, S. Parkins, and B. Dayan, Physical Review A **84**, 033854 (2011).
[7] N. H. Lindner and T. Rudolph, Physical Review Letters **103**, 113602 (2009).
[8] I. Schwartz, D. Cogan, E. R. Schmidgall, Y. Don, L. Gantz, O. Kenneth, N. H. Lindner, and D. Gershoni, Science **354**, 434 (2016).
[9] A. Imamoglu, D. D. Awschalom, G. Burkard, D. P. DiVincenzo, D. Loss, M. Sherwin, and A. Small, Physical Review Letters **83**, 4204 (1999).
[10] T. Wilk, S. C. Webster, A. Kuhn, and G. Rempe, Science **317**, 488 (2007).
[11] N. Somaschi, V. Giesz, L. De Santis, J. C. Loredo, M. P. Almeida, G. Hornecker, S. L. Portalupi, T. Grange, C. Antón, J. Demory, C. Gómez, I. Sagnes, N. D. Lanzillotti-Kimura, A. Lemaître, A. Auffeves, A. G. White, L. Lanco, and P. Senellart, Nature Photonics **10**, 340 (2016).
[12] X. Ding, Y. He, Z.-C. Duan, N. Gregersen, M.-C. Chen, S. Unsleber, S. Maier, C. Schneider, M. Kamp, S. Höfling, C.-Y. Lu, and J.-W. Pan, Physical Review Letters **116**, 020401 (2016).
[13] H. Wang, Y.-M. He, T.-H. Chung, H. Hu, Y. Yu, S. Chen, X. Ding, M.-C. Chen, J. Qin, X. Yang, et al., Nature Photonics , 1 (2019).
[14] C. Y. Hu, W. J. Munro, and J. G. Rarity, Physical Review B (Condensed Matter and Materials Physics) **78**, 125318 (2008).
[15] L.-M. Duan and H. J. Kimble, Physical Review Letters **92**, 127902 (2004).
[16] D. E. Chang, V. Vuletić, and M. D. Lukin, Nature Photonics **8**, 685 (2014).
[17] S. E. Economou, N. Lindner, and T. Rudolph, Physical review letters **105**, 093601 (2010).
[18] H. Pichler, S. Choi, P. Zoller, and M. D. Lukin, Proceedings of the National Academy of Sciences **114**, 11362 (2017).
[19] M. T. Rakher, N. G. Stoltz, L. A. Coldren, P. M. Petroff, and D. Bouwmeester, Phys. Rev. Lett. **102**, 097403 (2009).
[20] V. Loo, C. Arnold, O. Gazzano, A. Lemaitre, I. Sagnes, O. Krebs, P. Voisin, P. Senellart, and L. Lanco, Physical Review Letters **109**, 166806 (2012).
[21] P. Hilaire, C. Antón, C. Kessler, A. Lemaître, I. Sagnes, N. Somaschi, P. Senellart, and L. Lanco, Applied Physics Letters **112**, 201101 (2018).
[22] A. Dousse, L. Lanco, J. Suffczyński, E. Semenova, A. Miard, A. Lemaître, I. Sagnes, C. Roblin, J. Bloch, and P. Senellart, Physical Review Letters **101**, 267404 (2008).
[23] A. K. Nowak, S. L. Portalupi, V. Giesz, O. Gazzano, C. Dal Savio, P. F. Braun, K. Karrai, C. Arnold, L. Lanco, I. Sagnes, A. Lemaître, and P. Senellart, Nat Commun **5**, 3240 (2014).
[24] J. H. Prechtel, A. V. Kuhlmann, J. Houel, A. Ludwig, S. R. Valentin, A. D. Wieck, and R. J. Warburton, Nature Materials **15**, 981 (2016).
[25] H. Drexler, D. Leonard, W. Hansen, J. Kotthaus, and P. Petroff, Physical Review Letters **73**, 2252 (1994).
[26] R. J. Warburton, C. Schäflein, D. Haft, F. Bickel, A. Lorke, K. Karrai, J. M. Garcia, W. Schoenfeld, and P. M. Petroff, Nature **405**, 926 (2000).
[27] P.-L. Ardelt, T. Simmet, K. Müller, C. Dory, K. Fischer, A. Bechtold, A. Kleinkauf, H. Riedl, and J. Finley, Physical Review B **92**, 115306 (2015).
[28] M. Pooley, D. Ellis, R. Patel, A. Bennett, K. Chan, I. Farrer, D. Ritchie, and A. Shields, Applied Physics Letters **100**, 211103 (2012).

[29] M. Reindl, J. H. Weber, D. Huber, C. Schimpf, S. F. Covre da Silva, S. L. Portalupi, R. Trotta, P. Michler, and A. Rastelli, arXiv e-prints , arXiv:1901.11251 (2019), arXiv:1901.11251 [cond-mat.mes-hall].
[30] T. Sosnowski, T. Norris, H. Jiang, J. Singh, K. Kamath, and P. Bhattacharya, Physical Review B **57**, R9423 (1998).
[31] M. Bayer, S. Walck, T. Reinecke, and A. Forchel, Physical Review B **57**, 6584 (1998).
[32] M. Bayer, G. Ortner, O. Stern, A. Kuther, A. A. Gorbunov, A. Forchel, P. Hawrylak, S. Fafard, K. Hinzer, T. L. Reinecke, S. N. Walck, J. P. Reithmaier, F. Klopf, and F. Schäfer, Physical Review B **65**, 195315 (2002).
[33] M. Ediger, G. Bester, A. Badolato, P. Petroff, K. Karrai, A. Zunger, and R. Warburton, Nature Physics **3**, 774 (2007).
[34] M. Ediger, G. Bester, B. Gerardot, A. Badolato, P. Petroff, K. Karrai, A. Zunger, and R. Warburton, Physical review letters **98**, 036808 (2007).
[35] V. Mlinar and A. Zunger, Physical Review B **80**, 035328 (2009).
[36] H. Kamada, H. Gotoh, J. Temmyo, T. Takagahara, and H. Ando, Physical Review Letters **87**, 246401 (2001).
[37] Y.-M. He, Y. He, Y.-J. Wei, D. Wu, M. Atature, C. Schneider, S. Hofling, M. Kamp, C.-Y. Lu, and J.-W. Pan, Nature Nanotechnology **8**, 213 (2013).
[38] V. Giesz, N. Somaschi, G. Hornecker, T. Grange, B. Reznychenko, L. De Santis, J. Demory, C. Gomez, I. Sagnes, A. Lemaître, et al., Nature Communications **7**, 11986 (2016).
[39] B. Piętka, J. Suffczyński, M. Goryca, T. Kazimierczuk, A. Golnik, P. Kossacki, A. Wysmolek, J. Gaj, R. Stępniewski, and M. Potemski, Physical Review B **87**, 035310 (2013).
[40] R. Dahbashi, J. Hübner, F. Berski, K. Pierz, and M. Oestreich, Physical review letters **112**, 156601 (2014).
[41] R. H. Brown and R. Twiss, Proceedings of the Royal Society of London. Series A. Mathematical and Physical Sciences **243**, 291 (1958).
[42] C. K. Hong, Z. Y. Ou, and L. Mandel, Physical Review Letters **59**, 2044 (1987).
[43] J. Loredo, C. Antón, B. Reznychenko, P. Hilaire, A. Harouri, C. Millet, H. Ollivier, N. Somaschi, L. De Santis, A. Lemaître, et al., Nature Photonics , 1 (2019).